Variability in G-Protein-Coupled Signaling Studied with Microfluidic Devices

Xiaoyan Robert Bao,[†§*] Iain D. C. Fraser,[‡] Estelle A. Wall,[‡¶] Stephen R. Quake,[‖] and Melvin I. Simon[‡¶]

[†]Department of Applied Physics and [‡]Division of Biology, California Institute of Technology, Pasadena, California; [§]Center for Human Genetics Research, Massachusetts General Hospital, Boston, Massachusetts; [¶]Department of Pharmacology, University of California at San Diego, La Jolla, California; and [‖]Department of Bioengineering, Stanford University, Stanford, California

ABSTRACT Different cells, even those that are genetically identical, can respond differently to identical stimuli, but the precise source of this variability remains obscure. To study this problem, we built a microfluidic experimental system which can track responses of individual cells across multiple stimulations. We used this system to determine that amplitude variation in G-protein-activated calcium release in RAW264.7 macrophages is generally extrinsic, i.e., they arise from long-lived variations between cells and not from stochastic activation of signaling components. In the case of responses linked to P2Y family purine receptors, we estimate that approximately one-third of the observed variability in calcium release is receptor-specific. We further demonstrate that the signaling apparatus downstream of P2Y6 receptor activation is moderately saturable. These observations will be useful in constructing and constraining single-cell models of G protein-coupled calcium dynamics.

INTRODUCTION

Many macroscopic events in the life of a mammal, from development to T cell recruitment to carcinogenesis, arise from events occurring in a single cell. To quantitatively understand these processes, one needs to determine not just average behaviors for a given cell population, but also the distribution of behaviors in single cells. It is well established that individual mammalian cells within a supposedly homogenous culture can vary widely in their signaling responses to external stimuli. In addition, in several instances of note, the underlying distributions of single-cell behavior look quite different from their bulk averages (1,2).

Recent studies of variability in mammalian cell signaling have used either long-lived protein-level changes that could be observed with multiparameter flow cytometry (3), or the use of matched daughter cells (4) as effective copies of the same system. However, the former technique cannot observe transient signaling events, while the latter by itself does not provide information as to the molecular basis of signaling variation. We show in this work that both of these pitfalls can be avoided by observing cells under rapid, sequential stimulation. Applying two identical stimuli in rapid succession and then correlating responses on a cell-by-cell basis allows long-lived variations in signaling sensitivity to be discerned from stochastic noise that is different for every response. In this mode, the experiment is the direct signaling equivalent of two-color protein synthesis experiments used to study noise in protein synthesis (5). In addition, we show that correlating responses of individual cells to different stimuli provides information on the specific molecular contributors to signaling variation.

We used microfluidic devices to effect the requisite switching of solutions for such experiments. Microfluidic devices have been used in a broad range of applications in cell biology, most prominently for their ability to perform biochemical analyses on single cells (6–9) and their ability to generate novel physical environments, such as stable gradients, for the study of physiology (10,11). In this study, we have used microfluidics to combine precise timing control with integration of multiple simultaneous experiments into one field of view in the microscope. This latter feature allowed us to rule out effects of subpopulational variability (12), wherein samples of the same cell culture have been observed to perform differently at different times, when interpreting our data.

We used our experimental system to study variability in G-protein signaling-induced calcium release in RAW264.7 macrophages. Briefly, at the plasma membrane of a mammalian cell, an activated G-protein-coupled receptor (GPCR) effects the exchange of GTP for GDP in a heterotrimeric G-protein, causing the G-protein to dissociate into the α-subunit and the $\beta\gamma$ complex. Either dissociation product may activate phospholipase C (PLC), which cleaves phosphatidylinositol 4,5-diphosphate to release inositol 1,4,5-triphosphate (IP3). The IP3 then diffuses to the endoplasmic reticulum and binds to its cognate receptor, IP3R, which allows release of calcium from the ER store into the cytoplasm as a second messenger. Calcium release can be measured easily using standard fluorescence microscopy techniques, and several groups have demonstrated measurements of variability in single cell calcium dynamics using microfluidic devices (13–15).

Submitted November 3, 2009, and accepted for publication August 24, 2010.

*Correspondence: bao@chgr.mgh.harvard.edu

Iain D. C. Fraser's present address is Program in Systems Immunology and Infectious Disease Modeling (PSIIM), National Institute of Allergy and Infectious Diseases, National Institutes of Health, Bethesda, MD.

Editor: Andre Levchenko.

0006-3495/10/10/2414/9 $2.00

doi: 10.1016/j.bpj.2010.08.043

We observed that, for all the ligands that we have tested, most of the associated signaling variability arises from long-lived cell state differences and not from stochasticity in the signal transmission process. Cell-state differences persist, at least, for hours, and likely involve differences in either protein expression levels or protein-protein interactions. We then focused on signaling through members of the P2Y family of purine receptors, and estimated that approximately one-third of the variability in signal transmission in those receptors is directly associated with the cognate receptor. Finally, we obtained evidence suggesting that the P2Y6 receptors can partially saturate their downstream signaling partners. Our experimental platform offers a path to identify specific molecular contributors to signaling variability. Moreover, our results here both validate existing modeling of populational calcium response, and provide insights into how to build single-cell versions of calcium response models.

MATERIALS AND METHODS

Materials and Methods may be found in the Supporting Material.

RESULTS

Device design

Data presented in this article were obtained using two different microfluidic device designs, shown in Fig. 1, *a* and *b*, built around a common central core which is displayed in greater detail in Fig. 1 *c*. The devices use integrated microvalves to gate flow within the flow layer.

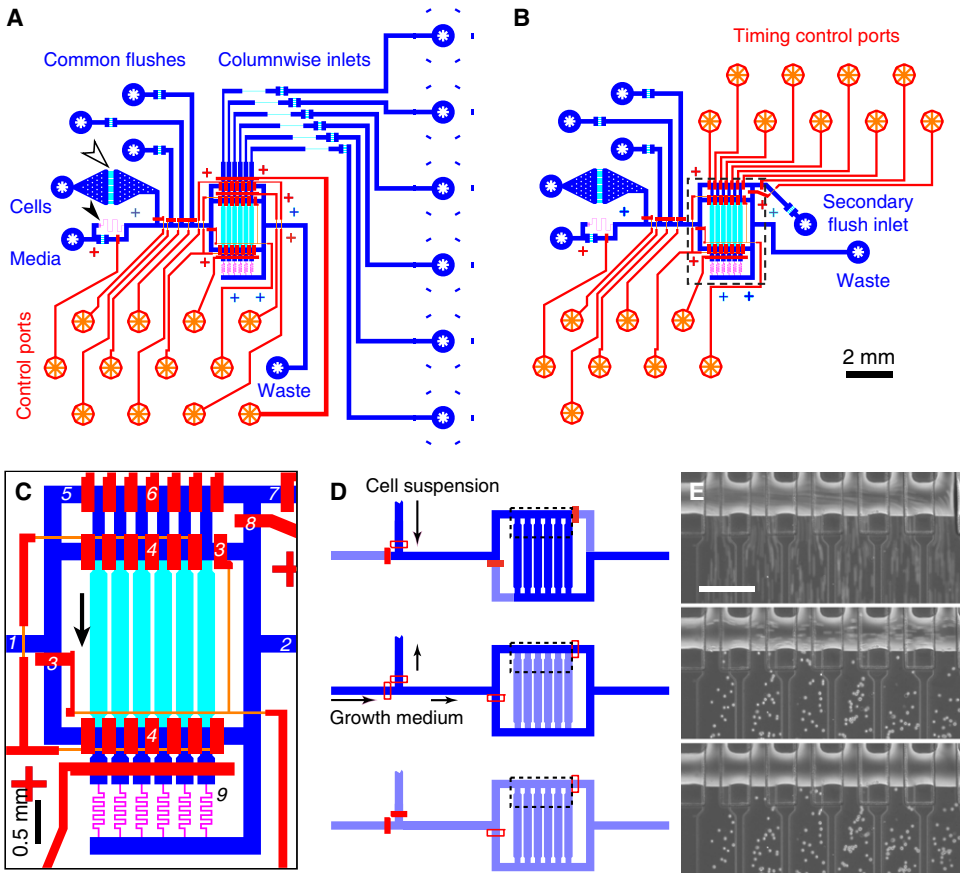

FIGURE 1 Device design and seeding. In panels *A–C*, flow layer features are in cool tones, with rounded features (45 μm peak height) in dark blue, unrounded high features (25 μm) in light blue, and unrounded low features (10 μm) in violet. Control layer features, all unrounded, are shown in warm tones, either red (high features, 40 μm) or yellow (low features, 10 μm), overlaid atop the flow layer features. (*A*) Design of the differential perfusion device, with one inlet for each cell channel. The media inlet flow resistor (*solid arrowhead*) allows very slow perfusion of the device, and the cell strainer (*outlined arrowhead*) traps cell clumps that may otherwise clog the device. (*B*) Design of the differential timing device, with additional control lines to apply solutions at different times for the different cell channels. (*C*) Expanded version of the central structure in panel *B*; the corresponding region of panel *A* is very similar. Cells reside within the set of six high, unrounded channels (flow direction indicated by the *black arrow*). Numbered device features are as follows: 1. Main inlet into the central structure, which delivers cells, media, stimulating ligands, etc. 2. Waste outlet. 3. Bypass valves used in cell injection (see panel *D*). 4. Channel isolation valves, actuated once cells are injected. 5. Inlet shunt, which allows direct connection of solution from main inlet into waste port. 6. Separation valves that determine which channels are perfused from the left and which from the right. 7. Secondary inlet and valve, used to supply right-side channels during timing experiments (see Fig. S1 *f*). 8. Shunt for secondary inlet. 9. Thin, serpentine channels used to balance flow rates across channels, along with corresponding access valve. Details on how these features are used can be found in Fig. S1. (*D* and *E*) Scheme *D* and corresponding images in panel *E* for loading channels with cells while avoiding crushing damage to cells. The region of the device imaged in panel *E* is shown in dotted outline in panel *D*. Scale bar in panel *E* is 300 μm. All flow features in panel *D* are shown in blue, with darker blue indicating channels with fluid flowing and lighter blue indicating channels where flow is expected to be stagnant. Some control valves, and all associated connecting channels, have been omitted for clarity. Cell suspension is initially injected into the central cross channels (*top*). Note that the lengths of particle streaks in the image indicate relative flow velocities. Once channels are seeded with cells, flow is diverted to bypass channels by opening the appropriate valves, at which point the entire device can be flushed with clean media (*middle*) without washing cells out of the cross channels. Once the peripheral channels are washed clean of cells, flow can be shut off entirely (*bottom*) to allow cells to adhere.

An array of six channels holds cells for culturing and stimulation, with outlets that go to the waste port and inlets that could be connected to a common inlet manifold. Flow constrictions upstream and downstream moderate and equalize flow rates, in direct analogy to the use of resistors in electrical circuits. In addition, one version of the device (Fig. 1 *a*) allows each cell channel to be connected to an individual inlet port, and the other (Fig. 1 *b*) allows channels to be connected to inlet ports either on the left or on the right, allowing for alternate solution flushes that could sweep across the device with defined timings. A detailed description of these procedures appears as Fig. S1 in the Supporting Material.

Cell injection and culturing

The use of integrated microvalves within devices demanded control over cell positioning, because otherwise cells within an actuating valve would be crushed, releasing their contents, which could contaminate downstream experiments. Other groups have used protein micropatterning to determine placement of cells, but preventing adhesion of RAW264.7 cells is difficult due to the presence of macrophage scavenger receptors. Instead, we controlled cell placement using hydrodynamics, with a structure analogous to electrical bridge circuits (16) that allowed us to seed cells into the central array of channels and then wash cells out of the rest of the device with clean media. The injection scheme and corresponding pictures demonstrating its implementation are shown in Fig. 1, *d* and *e*, and a movie of the injection process is available as Movie S2 in the Supporting Material. This seeding technique is fast, requiring only ~1 h to prepare and seed the device, and very general, dependent only on the ability to prepare a suspension of single cells which can adhere to channel walls. In addition to cells of the RAW264.7 macrophage cell line, we have injected and cultured bone marrow-derived macrophages and HEK293 cells. After designing and validating our injection scheme, we learned of cell microtraps (14,17), which are another solution to the problem of retaining cells within parts of the device while the rest is washed clear of cells. We note that we regularly observed at least three times as many cells per unit area as can be trapped in such cell arrays, due to the device area consumed by the traps themselves and the need for gaps between traps to allow fluid flow.

Cells were cultured either with constant perfusion at 0.07 μL/h/channel (5 μm/s linear velocity in the middle of the channel), or intermittent perfusion at 0.5 μL/h/channel (40 μm/s) for 1 min out of every hour. The higher flow rate corresponds to 0.06 dyne/cm^2, well below shear stresses of physiological relevance. During cell staining and stimulation, flushes occurred at ~1.5 dyne/cm^2 (0.9 mm/s). Cells experienced the most shear, ~12 dyne/cm^2 (7.5 mm/s), briefly during the initial application of ligands; this shear stress has been known to elicit physiological responses. However, there was little difference in responses between cells near the center of the channels, where the shear stress was highest, and cells near the channel walls, which were more protected from flow shear (Fig. S3). In addition, we observed no calcium responses when cells were mock-stimulated with assay media devoid of ligands. We therefore conclude that the shear forces to which cells were exposed did not compromise our calcium data.

In addition to the presence of shear flow, conditions within our microfluidic system differ from standard cell culturing conditions in terms of media volume per cell: ~20 pL per cell in our devices versus ~1 nL per cell in a tissue culture plate. Thus, we considered the possibility that they might deplete metabolites during culturing. Precise metabolic data for RAW264.7 cells are unavailable, but oxygen consumption of RAW cells has been measured at 115 fmol O_2 per cell per hour (18), implying glutamine (19) and glucose consumption rates that both intermittent and continuous perfusion are able to support. Oxygen availability itself is not expected to limit cellular growth due to the high gas permeability of our microfluidic devices. Further, the amount of amino acids present in a channelful of medium is expected to be sufficient to support protein synthesis for >1 h. While it is possible that other factors in the media, such as vitamins or serum components, will become limiting for cell growth, we observed normal calcium responses for cells grown in devices overnight with intermittent perfusion (compare Fig. S7 with Fig. 4 *a*), so any such effects are not expected to strongly affect calcium signaling.

Observation of calcium dynamics

We performed live-cell calcium imaging studies of RAW264.7 macrophage cells stimulated with GPCR ligands. Fig. 2 shows the results of typical experiments of calcium release in RAW cells arising from stimulation with the nucleotide uridine 5′-diphosphate (UDP). Each cell-bearing channel in the device could be treated with a different concentration of UDP. Channels contained between 100 and 300 cells each, and could be stimulated identically to obtain more statistical power when necessary.

While entire time courses were taken of all cells (Fig. 2 *a*), we limit ourselves here to analyzing the peak rise in cytosolic calcium above the prestimulus baseline value. We used the magnitude of the maximal rise in calcium concentration, rather than the peak calcium concentration itself, because often the changes in calcium concentration were of similar or smaller magnitude than the baseline calcium concentration; quoting the absolute calcium concentrations would have implied a response where none existed. Henceforth the terms calcium response and calcium response amplitude shall always denote the peak change in calcium level in response to agonist. Using this metric, we obtained dose-response results from a typical

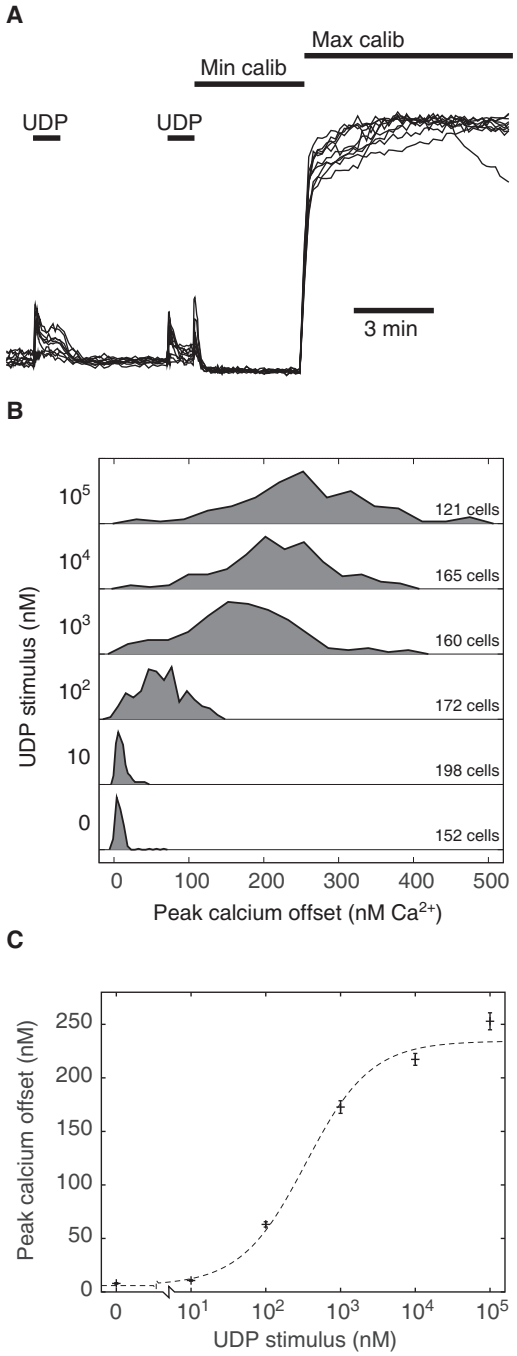

FIGURE 2 Observations of calcium signaling in RAW264.7 macrophages upon UDP stimulation. (*A*) Intensity time traces of 10 cells chosen at random from a typical experiment. Cells were stimulated twice with ligands, after which they were treated with calibration solutions (see Materials and Methods) to allow correction for variations in staining and background fluorescence. Traces shown were individually rescaled according to their minimum and maximum calibration intensities. (*B*) Response distributions to a series of UDP doses obtained from one single experiment. (*C*) Dose-response curve for data in panel *B*. Error bars shown here are mean ± SE of individual cell values over the populations being observed. (*Dashed line*) Best fit line, with $K_d = 343 \pm 73$ nM.

experiment (Fig. 2 *c*) that gave an EC_{50} of 343 ± 73 nM, comparable to those reported in the literature for IP3 release arising from P2Y6 receptor activation (300 nM; (20)), and in addition gave response population distributions (Fig. 2 *b*) that are typically inaccessible in bulk experiments.

Kinetic experiments

Our microfluidic devices allowed us to perform repeated stimulations of cells. However, to be able to compare a cell's responses to two different stimuli, we first needed to ensure that the cell is able to fully recover from the first stimulus before applying the second. UDP stimulation triggers a strong release of calcium stores, so we were interested in the recovery of those stores after ligand washout. Fig. 3, *a* and *b*, show that the stores generally recover within 2–3 min, so we set the interstimulus washout time to 4 min. Further experimentation showed that recovery of the calcium response amplitude followed similar kinetics (data not shown). We wished to further minimize effects of the

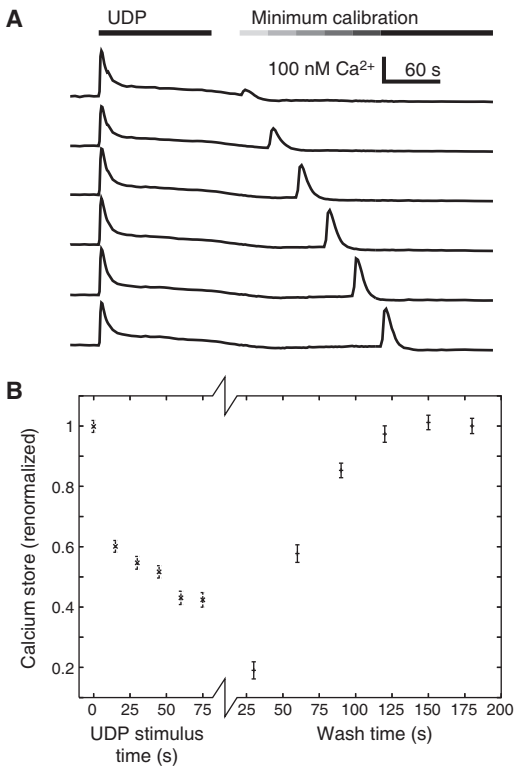

FIGURE 3 Kinetics measurements. (*A*) Series of raw kinetics traces demonstrating cellular calcium pool recovery. The transient rise in calcium during the minimum calibration phase is due to ER calcium release induced by thapsigargin (see Materials and Methods), and the strength of that rise scales with the amount of calcium in ER stores. (*B*) Kinetics of calcium depletion and recovery upon stimulation with UDP. Plotted on the *y* axis are the areas under the thapsigargin-induced calcium traces. Analyzed data from panel *A* are plotted on the right; data for the left side of the plot were obtained similarly, integrating thapsigargin-induced peaks in an experiment which varied the duration of UDP exposure between 0 and 75 s.

initial stimulus by shortening it, but measurement of the time course of calcium store depletion showed that most of the store depletion occurs during the first 15 s of the calcium response (Fig. 3 *b*). Because calcium responses could peak rather slowly with lower ligand doses or lower cellular responsiveness, we chose a stimulation time of 60 s.

During the recovery experiments, we noticed that subsequent calcium response amplitudes tended not to recover to 100% of the response amplitudes to the initial stimulus, though they usually did reach between 80% and 90%. This effect was observed for all nucleotide ligands used in this work. We wondered if the effect indicated receptor desensitization (reviewed in (21)), and indeed we were able to measure desensitization kinetics of the receptor to the anaphylatoxin C5a in RAW264.7 cells. That the decrease in C5a responses seen in our experiments is indeed receptor desensitization is confirmed by observation of slower kinetics upon RNAi knockdown of the G receptor kinases (GRKs) responsible for initiation of the receptor desensitization mechanism ((22) Fig. S4). However, desensitization of P2Y receptors has not been reported in RAW264.7 macrophages, and such desensitization did not appear to occur in our experiments. We tested this by comparing two sets of cells in the same device, of which only one set underwent the initial stimulation. The response amplitudes of the two sets of cells to the second stimulation were not significantly different (Fig. S5). Our interpretation of the mild reduction seen in calcium response amplitudes is that some part of the experiment, perhaps photobleaching of calcium indicator, gradually reduces the amplitude of cellular calcium responses in a general way. This effect is independent of the stimulus applied to cells, and small enough that it does not greatly alter the correlation between different rounds of stimulus (see below).

In support of this interpretation, we found that channel-to-channel variability was magnified in those experiments where each channel was stimulated at a different time (Fig. S6). The changing cellular physiology over short time periods underscores the necessity of performing matched controls in parallel with experiments.

Correlating sequential responses

To establish the repeatability of calcium responses, we first rechallenged the cells with exactly the same stimulus. Calcium responses to identical stimulations were always well correlated (usually $r \approx 0.9$) on a cell-by-cell basis (Fig. 4, *a–c*; Table S8). This clearly demonstrates that cell-to-cell GPCR signaling variation arises from variations in cellular state, such as protein expression levels, rather than stochasticity in the signal transmission process (5). We note that this is not unexpected, because none of the molecular species in the signal transduction pathway are expected to be present at copy numbers <1000 (23), and has been observed in other cell lines (24).

This observation appears to be independent of the G-protein coupling of the cognate receptors, and independent of the desensitization. First and second responses, when they were to the same ligand, were well correlated for all ligands tested: the nucleotides UDP, uridine 5′-triphosphate (UTP), and adenosine 5′-triphosphate (ATP), whose cognate receptors couple to PLCβ via $G_{\alpha q/11}$ and

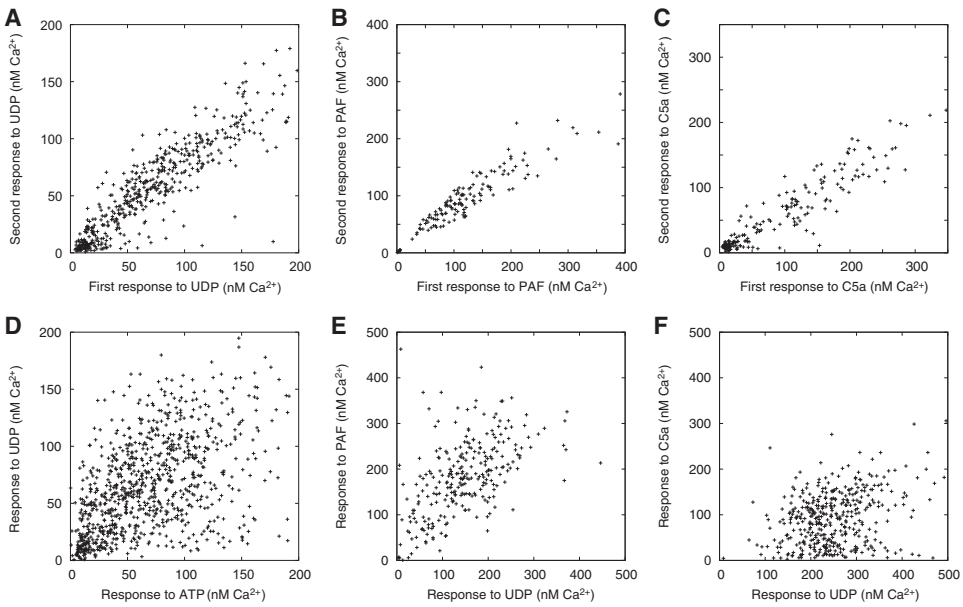

FIGURE 4 Scatter plots showing single-cell calcium response amplitudes to ligands in sequential stimulation experiments. In all cases, cells were treated with the first stimulus for 1 min, washed with assay buffer for 4 min, and treated with the second stimulus for 1 min before being treated with calibration solutions. Each data point in these scatter plots corresponds to a single cell, with the two calcium response amplitudes plotted on the two axes; calcium response amplitudes for the first stimulation are always plotted on the *x* axis. (*A–C*) Repeated stimulations, using three different ligands. UDP was used at 1 μM, PAF at 10 nM, and C5a at 250 nM. Correlation coefficients are all close to 0.9. (*D–F*) Double stimulations using different ligands. (*D*) Much lower correlations between UDP (first stimulus; 1 μM) and ATP (second stimulus; 1 μM) response amplitudes, with a correlation coefficient of $r \approx 0.51$. ATP was supplemented here with 3 mM EDTA (see text). (*E*) Correlation between UDP (first stimulus; 10 μM) and PAF (second stimulus; 100 nM) is $r \approx 0.52$. (*F*) Correlation between UDP (first stimulus; 10 μM) and C5a (second stimulus; 250 nM) is much lower: $r \approx 0.30$. (For further information, see Table S8.)

do not desensitize; platelet-activating factor (PAF), which couples predominantly via $G_{\alpha q/11}$ but does desensitize (25); and C5a, which couples to $G_{\alpha i}$ (26) and is known to desensitize via receptor phosphorylation and internalization. Correlation data for the nucleotides are summarized in Table 1, and data for all ligands are shown in Table S8. The low degree of intrinsic signaling variation thus appears to be a general phenomenon. The strong correlations observed here also indicate that the slow signal response reductions noted in the previous subsection do not contribute appreciably to the variability in calcium responses.

Because the cells in our devices were subjected to strong confinement, it was in principle possible that much of the observed variations in signaling arose from variations in local conditions to which cells were exposed. These variations could be, for instance, in metabolite or signaling molecule concentrations, or in the degree or nature of cell-to-cell contacts. To understand the nature of the observed signaling variation, we cultured cells for 24 h in our device and tracked cell divisions, so that we could identify both daughter cells from individual cell division events and then correlate their calcium responses. As in the case of apoptotic signaling (4), responses of sister cells correlated strongly. At the same time, we could consider all pairs of cells closer together than the mean daughter cell pair, and doing so abolishes the observed response correlation (Fig. S7).

Signaling variation could also occur over longer distances, because upstream cells may secrete or deplete factors that affect the physiology of downstream cells. We tested for the influence of these effects by comparing calcium responses in cells in the upstream one-third of channels against responses in cells in the downstream one-third. Using the Mann-Whitney signed rank test for both first and second responses in all the experiments listed in Table S8, we found significant ($p < 0.05$) differences in nine of 58 such comparisons. Within those comparisons, linear regression of responses against cells' positions along the channels gave correlation coefficients $r^2 > 0.02$ in only one experiment; removing those data from our analysis does not change any of the conclusions (Table S8). If we assume that effects observed here extrapolate linearly with channel length, then the correlation coefficients r^2 should scale as the square of the channel length. Thus, differences between upstream and downstream cells may potentially become significant contributors to overall signaling variance ($r^2 > 0.1$) as the length of channel under observation increases beyond twice that of the present experiments (i.e., >2.6 mm). We are actively working on altering the design of our devices to explore this issue.

TABLE 1 Correlations between responses to nucleotides

	UTP	UDP	ATP
UTP	0.889 ± 0.013	0.638 ± 0.040	0.843 ± 0.004
UDP		0.903 ± 0.007	0.564 ± 0.031
ATP			0.902

Mean correlation coefficients (r) across different experiments, along with associated standard errors (n between 3 and 5, except for the ATP-ATP experiment, which we only performed once). Correlations were averaged without regard to order of ligand application. Ligand doses were either 1 or 2 μM; both doses are expected to saturate the cognate receptors without cross-activation of other receptors. ATP stimulation was in the presence of 3 mM EDTA, to prevent entry of extracellular calcium via P2X channels (34). See Table S8 for a detailed breakdown of the data.

The correlation between calcium responses of sister cells, the lack of such correlation between neighboring cells, and the paucity of apparent differences between upstream and downstream cells, argue strongly that inherent, cell-to-cell differences in protein levels and configurations, and not differences in environmental conditions, underlie the observed variations in calcium responses. The observed cell division events occurred an average of 16 h before stimulation, so cell state differences must persist for at least that length of time.

That the calcium responses were consistent across consistent stimuli allowed us to explore further the source of signaling variation. We stimulated cells first with ATP and then with UDP. Cognate receptors for both ligands couple through $G_{\alpha q/11}$ (26,27). Thus, any differences between responses to these two ligands must arise from differences that are directly associated with their cognate receptors. As shown in Fig. 4 *d*, responses to these two ligands were much less correlated with each other; $r \approx 0.6$. Additionally, the UDP responses were similarly correlated with another ligand that signals through $G_{\alpha q/11}$ ($r \approx 0.6$ between UDP and PAF; Fig. 4 *e*), and much less with one that signals through $G_{\alpha i}$ ($r \approx 0.3$ between UDP and C5a; Fig. 4 *f*).

We then systematically analyzed correlations between responses to the nucleotides ATP, UDP, and UTP, all of which signal via P2Y family receptors. To maximize response amplitudes while controlling for receptor cross-reaction, we used ligand concentrations that were modestly higher than their K_d values. Correlations are shown in Table 1 and Table S8, and the strong correlation between ATP and UTP corresponds nicely to the known ability of both P2Y2 and P2Y4 to respond to either ligand.

That ATP and UDP signal almost entirely through distinct receptors—ATP through P2Y2 and P2Y4 (27), and UDP through P2Y6 (28)—which couple to identical downstream effectors allows us to estimate the fraction of signaling noise contributed by receptor-specific effects. Consider two random variables, Y and Z, that describe the observed single-cell responses to two different ligands. We can decompose these into a common source of variation, x; separate, receptor-specific contributions, y and z; and signaling stochasticity δ,

$$\begin{cases} Y = x + y + \delta_Y \\ Z = x + z + \delta_Z \end{cases}.$$

Then the correlation coefficient between the two random variables is

$$r_{YZ} = \frac{\langle YZ\rangle - \langle Y\rangle\langle Z\rangle}{\sqrt{\mathrm{var}(Y)\mathrm{var}(Z)}},$$

where var(…) denotes the variance of the bracketed quantity. To obtain a rough estimate of the underlying variances, we approximate that x, y, and z are all uncorrelated with each other, and that $\mathrm{var}(y) \approx \mathrm{var}(z)$ and $\mathrm{var}(\delta_Y) \approx \mathrm{var}(\delta_Z)$. This gives, simply,

$$\begin{cases} r_{YZ} \approx \frac{\mathrm{var}(x)}{\mathrm{var}(x)+\mathrm{var}(z)+\mathrm{var}(\delta)} \\ r_{ZZ} \approx \frac{\mathrm{var}(x)+\mathrm{var}(z)}{\mathrm{var}(x)+\mathrm{var}(z)+\mathrm{var}(\delta)}, \end{cases}$$

where r_{ZZ} is the correlation between the first and second responses when they are to the same stimulus. Therefore, the fraction of cell-to-cell intrinsic variability attributable to receptor-specific effects is

$$\frac{\mathrm{var}(z)}{\mathrm{var}(x) + \mathrm{var}(z)} \approx 1 - \frac{r_{YZ}}{r_{ZZ}}.$$

Comparing calcium response amplitudes to UDP stimulus with those to ATP stimulus, we obtain an estimate of ~38% (close to one-third) contribution from receptor-specific sources.

Because the expected source of signaling noise is downstream of the receptors, rather than in parallel, one may make the argument that the contributions multiply instead of add. For instance, at a given ligand dose, there might be independent variation in 1), the number of receptors activated; and 2), the amount of calcium released by each receptor. In this case we have $Y = xy$ and $Z = xz$ (ignoring the small contributions from signaling stochasticity), and the above analysis can be applied to correlations between log-transformed data. Interestingly, modifying the analysis in this way does not change the correlation coefficients markedly (Table S8).

Downstream saturation

Instead of stimulating the signal transduction system at different receptors, we could also stimulate the same receptor at different strengths, i.e., different agonist concentrations. If all of the cell-to-cell variability arose from receptor level variations, then each cell in this paired assay—with its unique amount of receptor—would constitute a different natural experiment on the dose-response relationship of the downstream signal transmission system. A few such assays could, in theory, provide enough information to reconstruct the entire downstream dose-response curve. The results so obtained would necessarily be indirect, but would have the advantage of being produced without any modifications to the system being observed.

Of course, downstream processes do contribute a large part of the signaling variability, and these are expected to confound our measurements of the downstream signaling system. Despite this potential problem, we still observed significant structure within our experimental results. One such experiment, stimulating cells with UDP first at 100 nM and then at 1 μM, is shown in Fig. 5. Note the clear curving of the response scatter plot, where cells that respond strongly to 100 nM of UDP do not greatly increase their responses when the stimulating UDP concentration is increased 10-fold. We hypothesized that this occurred because cells have a natural maximum calcium response amplitude. Those cells that express high amounts of receptor on their surfaces reach that maximum response with the lower dose of ligand, so that the increase in ligand dose on the second stimulation fails to increase the calcium response.

We used this downstream saturation hypothesis to derive a fitting function for the UDP response correlation data, and the optimized fit curve (shown) improves the fitting residuals significantly ($p < 10^{-10}$; see Materials and Methods). We observed statistically significant curving in the response scatter plots from all such experiments ($n = 3$; $p < 10^{-4}$ in all cases), including one where the order of the stimulations was reversed and the opposite curvature observed. The fits gave a maximal calcium response amplitude of 270 ± 56 nM Ca^{2+}, with a receptor activation ratio of 3.60 ± 0.75, corresponding to a half-saturating does of 448 ± 178 nM for P2Y6 receptor activation (all values

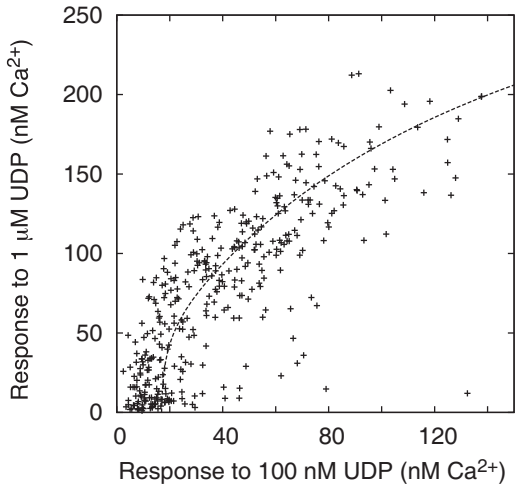

FIGURE 5 Scatter plot, similar to those shown in Fig. 4, showing responses to different doses of the same ligand. Cells were stimulated with 100 nM UDP for 1 min, washed for 4 min, and then stimulated with 1 μM UDP for 1 min. The scatter deviates significantly from a straight line passing through the origin, demonstrating clear nonlinearity in the responses. For instance, whereas cells that responded with 25 nM Ca^{2+} to stimulation at 100 nM UDP could respond almost fourfold higher to 1 μM UDP, those that responded with 120 nM Ca^{2+} to 100 nM UDP responded less than twofold higher to 1 μM UDP. Note that the x axis has been expanded relative to the y axis to emphasize the nonlinearity. Curved line here represents the best downstream saturation model fit (see Materials and Methods and Results).

shown here are mean ± SE). The half-saturating dose is marginally larger than the EC_{50} derived from our calcium release dose-response curve, consistent with the notion of saturation in the downstream signaling system contributing to saturation of the overall response.

DISCUSSION

Our experiment combined three features that allowed us to make novel observations of variability in G protein-coupled signaling.

First, we took advantage of the existence of G protein-coupled receptors that do not desensitize, so that any given cell's responses to multiple stimulations could be meaningfully compared.

Second, our use of microfluidic devices allowed us to deliver those stimulations within minutes of each other, eliminating possible confounding effects of transcriptional effects arising from the initial stimulus. The microfluidic devices, moreover, allowed rapid determination of optimal stimulation timings.

Third, we used a cell line that endogenously expresses multiple receptors which couple to identical molecules in the downstream pathway. This allowed us to determine the relative contributions of different parts of the signaling pathway to the observed signaling variability.

That our correlation results for nucleotide ligands matched closely to the known ligand specificities of their cognate receptors strongly supports the use of these correlations for determining the sources of signal transmission variability. Our results for nucleotides indicate that approximately one-third of this variability is directly associated with the ligand. We expect that this variability arises from variation in receptor expression levels, but note that that is not the only possible explanation. Because activated G proteins diffuse little before they become inactive again (29), differences in receptor colocalization with G proteins or PLCβs can also give rise to receptor-specific signaling variability. In addition, physical interactions between receptors may modulate function (30).

These different possibilities may be experimentally tractable using fluorescence labeling techniques. For instance, if suitable antibodies against P2Y receptors exist, these could be used to quantify receptor expression levels on cells at the end of calcium experiments or to characterize correlations between expression levels of different P2Y receptors on the cell population being studied. Fluorescent fusion protein expression is another possible experimental approach, though with the caveat that such experiments would alter receptor expression levels.

Implications for modeling efforts

Our experiments provide novel measurements of the response distribution of cell populations against which computational models of signaling may be evaluated. In particular, recent work on understanding the synergy between UDP and C5a in eliciting calcium release (23), if extended to consider single-cell variations, would be constrained because they would need to reproduce the correlations between UDP and C5a responses measured here.

One major caveat for quantitative modeling of averaged data in biological systems has been the potential for the underlying system to be highly nonlinear. This nonlinearity, in conjunction with cell-to-cell variability, has the potential to mask important effects that can only be resolved with single cell measurements (1). In this case, even though our data strongly suggest the presence of nonlinearity in the downstream G protein-triggered calcium response, the degree of nonlinearity is rather modest: downstream saturation only appears to have changed the EC50 of UDP by ~25%. Thus, saturation effects will likely not interfere strongly with existing modeling of bulk biochemical data (12,23).

Another insight from our results is that most of the variability seen in G-protein-coupled calcium release arises quite far upstream: even though C5a and UDP exhibit very similar PLCβ dependencies (26), their responses are quite poorly correlated. Therefore, when analyzing entire time courses instead of just peak responses, those peak responses can be used to narrow the search range of receptor and G protein levels, so that the shape of the subsequent response decay can be more effectively used to estimate other parameters in the signaling model. Our observations suggest that expression levels of downstream calcium-handling components are more consistent between cells; such a conclusion is partially corroborated by recent reports (24).

Finally, our data point to an interesting observation about variability in GRK expression levels. Recall that responses to repeated stimulations were strongly correlated even for stimulation with C5a, whose responses showed clear evidence of desensitization. Put another way, even though cells responded much more weakly to a second C5a stimulus, the ratio between the first and second responses was quite consistent, thereby giving a large correlation coefficient. Strong binding of C5a (31) probably contributes to this consistency. However, because C5a desensitization kinetics are slowed upon GRK knockdown (Fig. S4), consistency in calcium responses to C5a also suggests that there was little variation in GRK activity between different cells in our experiments. This observation will reduce the number of free parameters needed to model single cell behaviors in RAW264.7 macrophages.

CONCLUSIONS

Microfluidic devices provide unique opportunities to enhance the richness of single-cell data collected using microscopy. We have shown here that, in addition to engineering physical parameters of cells' environs (10,11,32,33), microengineered devices can also allow deep probing of signaling pathways by allowing multiple

stimulations on the same cells. We have used this technique to show that variability in G protein-coupled calcium release is mostly extrinsic, quantify the fraction of extrinsic variation that is receptor-specific, and infer that the signaling pathway downstream of receptor activation is saturable. While similar results may have been possible with perfusion flow cells, the inclusion of multiple different chambers within one microscope field of view allowed incorporation of matched control experiments that greatly eased interpretation of our data. At the same time, the constant perfusion allowed easy washout of ligands with little risk of carryover, which is difficult to achieve with automated plate-based assays. We believe the application of microfluidic technology will greatly enhance the richness, quality, and throughput of imaging-based signaling experiments.

SUPPORTING MATERIAL

Additional materials and methods, six figures, one table, and one movie are available at http://www.biophysj.org/biophysj/supplemental/S0006-3495(10)01038-6.

We thank members of the Simon laboratory for excellent technical assistance; and T. Squires, M. Diehl, M. Baym, D. Zhang, an anonymous referee, and members of the Quake group and the Alliance for Cell Signaling for helpful comments.

This work was funded in part by the National Institute of General Medical Sciences Glue Grant Initiative (No. U54 GM062114), and by a Senior Scholar award in Aging from the Ellison Medical Foundation to M.I.S. X.R.B. acknowledges support from the Fannie and John Hertz Foundation.

REFERENCES

1. Ferrell, Jr., J. E., and E. M. Machleder. 1998. The biochemical basis of an all-or-none cell fate switch in Xenopus oocytes. *Science.* 280:895–898.
2. Lahav, G., N. Rosenfeld, …, U. Alon. 2004. Dynamics of the p53-Mdm2 feedback loop in individual cells. *Nat. Genet.* 36:147–150.
3. Feinerman, O., J. Veiga, …, G. Altan-Bonnet. 2008. Variability and robustness in T cell activation from regulated heterogeneity in protein levels. *Science.* 321:1081–1084.
4. Spencer, S. L., S. Gaudet, …, P. K. Sorger. 2009. Non-genetic origins of cell-to-cell variability in TRAIL-induced apoptosis. *Nature.* 459:428–432.
5. Elowitz, M. B., A. J. Levine, …, P. S. Swain. 2002. Stochastic gene expression in a single cell. *Science.* 297:1183–1186.
6. Huang, B., H. Wu, …, R. N. Zare. 2007. Counting low-copy number proteins in a single cell. *Science.* 315:81–84.
7. Ottesen, E. A., J. W. Hong, …, J. R. Leadbetter. 2006. Microfluidic digital PCR enables multigene analysis of individual environmental bacteria. *Science.* 314:1464–1467.
8. Toriello, N. M., E. S. Douglas, …, R. A. Mathies. 2008. Integrated microfluidic bioprocessor for single-cell gene expression analysis. *Proc. Natl. Acad. Sci. USA.* 105:20173–20178.
9. Zhong, J. F., Y. Chen, …, L. P. Weiner. 2008. A microfluidic processor for gene expression profiling of single human embryonic stem cells. *Lab Chip.* 8:68–74.
10. Lucchetta, E. M., J. H. Lee, …, R. F. Ismagilov. 2005. Dynamics of *Drosophila* embryonic patterning network perturbed in space and time using microfluidics. *Nature.* 434:1134–1138.
11. Paliwal, S., P. A. Iglesias, …, A. Levchenko. 2007. MAPK-mediated bimodal gene expression and adaptive gradient sensing in yeast. *Nature.* 446:46–51.
12. Maurya, M. R., and S. Subramaniam. 2007. A kinetic model for calcium dynamics in RAW 264.7 cells. 1. Mechanisms, parameters, and subpopulational variability. *Biophys. J.* 93:709–728.
13. Wheeler, A. R., W. R. Throndset, …, A. Daridon. 2003. Microfluidic device for single-cell analysis. *Anal. Chem.* 75:3581–3586.
14. Faley, S., K. Seale, …, J. P. Wikswo. 2008. Microfluidic platform for real-time signaling analysis of multiple single T cells in parallel. *Lab Chip.* 8:1700–1712.
15. Schiffenbauer, Y. S., Y. Kalma, …, G. Berke. 2009. A cell chip for sequential imaging of individual non-adherent live cells reveals transients and oscillations. *Lab Chip.* 9:2965–2972.
16. Horowitz, P., and W. Hill. 1989. The Art of Electronics. Cambridge University Press, New York.
17. Di Carlo, D., L. Y. Wu, and L. P. Lee. 2006. Dynamic single cell culture array. *Lab Chip.* 6:1445–1449.
18. Nalwaya, N., and W. M. Deen. 2005. Nitric oxide, oxygen, and superoxide formation and consumption in macrophage cultures. *Chem. Res. Toxicol.* 18:486–493.
19. Reitzer, L. J., B. M. Wice, and D. Kennell. 1979. Evidence that glutamine, not sugar, is the major energy source for cultured HeLa cells. *J. Biol. Chem.* 254:2669–2676.
20. Communi, D., M. Parmentier, and J. M. Boeynaems. 1996. Cloning, functional expression and tissue distribution of the human $P2Y_6$ receptor. *Biochem. Biophys. Res. Commun.* 222:303–308.
21. Krupnick, J. G., and J. L. Benovic. 1998. The role of receptor kinases and arrestins in G protein-coupled receptor regulation. *Annu. Rev. Pharmacol. Toxicol.* 38:289–319.
22. Shin, K.-J., E. A. Wall, …, I. D. Fraser. 2006. A single lentiviral vector platform for microRNA-based conditional RNA interference and coordinated transgene expression. *Proc. Natl. Acad. Sci. USA.* 103:13759–13764.
23. Flaherty, P., M. L. Radhakrishnan, …, A. P. Arkin. 2008. A dual receptor crosstalk model of G-protein-coupled signal transduction. *PLOS Comput. Biol.* 4:e1000185.
24. Nakamura, N., T. Yamazawa, …, M. Iino. 2009. Temporal switching and cell-to-cell variability in Ca^{2+} release activity in mammalian cells. *Mol. Syst. Biol.* 5:247.
25. Izumi, T., and T. Shimizu. 1995. Platelet-activating factor receptor: gene expression and signal transduction. *Biochim. Biophys. Acta.* 1259:317–333.
26. Roach, T. I., R. A. Rebres, …, W. E. Seaman. 2008. Signaling and cross-talk by C5a and UDP in macrophages selectively use PLCβ3 to regulate intracellular free calcium. *J. Biol. Chem.* 283:17351–17361.
27. del Rey, A., V. Renigunta, …, P. J. Hanley. 2006. Knock-out mice reveal the contributions of P2Y and P2X receptors to nucleotide-induced Ca^{2+} signaling in macrophages. *J. Biol. Chem.* 281:35147–35155.
28. Nicholas, R. A., W. C. Watt, …, K. Harden. 1996. Uridine nucleotide selectivity of three phospholipase C-activating P2 receptors: identification of a UDP-selective, a UTP-selective, and an ATP- and UTP-specific receptor. *Mol. Pharmacol.* 50:224–229.
29. Ramanathan, S., P. B. Detwiler, …, B. I. Shraiman. 2005. G-protein-coupled enzyme cascades have intrinsic properties that improve signal localization and fidelity. *Biophys. J.* 88:3063–3071.
30. D'Ambrosi, N., M. Iafrate, …, C. Volonté. 2007. Comparative analysis of P2Y4 and P2Y6 receptor architecture in native and transfected neuronal systems. *Biochim. Biophys. Acta.* 1768:1592–1599.
31. Huey, R., and T. E. Hugli. 1985. Characterization of a C5a receptor on human polymorphonuclear leukocytes (PMN). *J. Immunol.* 135:2063–2068.
32. Hui, E. E., and S. N. Bhatia. 2007. Micromechanical control of cell-cell interactions. *Proc. Natl. Acad. Sci. USA.* 104:5722–5726.
33. Park, S., P. M. Wolanin, …, R. H. Austin. 2003. Motion to form a quorum. *Science.* 301:188.
34. Ralevic, V., and G. Burnstock. 1998. Receptors for purines and pyrimidines. *Pharmacol. Rev.* 50:413–492.